Hydrothermal Synthesis and Structural and Spectroscopic Properties of the New Triclinic Form of GdBO$_3$:Eu^{3+} Nanocrystals

Agata Szczeszak,[†] Tomasz Grzyb,[‡] Bolesław Barszcz,[†] Vitali Nagirnyi,[§] Aleksei Kotlov,[||] and Stefan Lis*,[‡]

[†]Institute of Molecular Physics, Polish Academy of Sciences, Mariana Smoluchowskiego 17, 60-179 Poznań, Poland
[‡]Department of Rare Earths, Faculty of Chemistry, Adam Mickiewicz University, Grunwaldzka 6, 60-780 Poznań, Poland
[§]Institute of Physics, University of Tartu, Riia 142, 51014 Tartu, Estonia
[||]HASYLAB at DESY, Gebaude 25b/309 Notkestr. 85, D-22607 Hamburg, Germany

Ⓢ Supporting Information
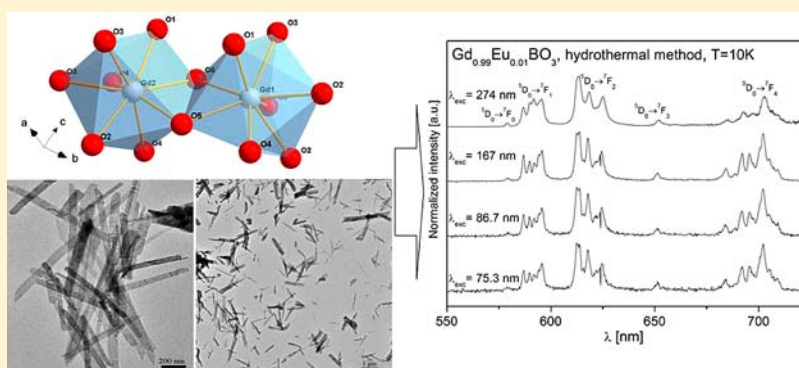
ABSTRACT: Triclinic Gd$_{1-x}$Eu$_x$BO$_3$ nanophosphors have been prepared by a hydrothermal method without using additional coreagents and prior precipitation of precursor (*in situ*). The formation of the borate nanorods and their crystal structure was refined on the basis of X-ray diffraction patterns (XRD) and well confirmed using various techniques such as infrared spectroscopy (IR), Raman spectroscopy, transmission electron microscopy (TEM), and energy-dispersive X-ray spectroscopy (EDX). The new triclinic crystal structure (space group $P\bar{1}$) for the GdBO$_3$ nanocrystals and detailed structure parameters were determined with the help of the Rietveld analysis. The spectroscopic characteristics of the synthesized nanomaterials with different concentrations of Eu^{3+} ions were defined with the use of luminescence excitation spectra as well as emission spectra and decay kinetics. The Judd–Ofelt parameters (Ω_2, Ω_4) and quantum efficiency, η, were also calculated for the more detailed analysis of Eu^{3+} spectra in the GdBO$_3$ host.

INTRODUCTION

Development of modern technology requires the creation of advanced materials with suitable physicochemical properties. Nowadays, this theme is very important due to still growing demand in the industry for advanced technologies and innovative materials. One of the most intensively developing technology fields is related to the synthesis and utilization of nanophosphors, e.g., aluminates, fluorides, oxyfluorides, or cerium–strontium oxides.[1−6] In recent years, much attention has been paid to rare earths orthoborate phosphors (REBO$_3$, RE = Y, La, Gd) due to their interesting spectroscopic properties, such as efficient emission of visible light under vacuum ultraviolet (VUV), ultraviolet (UV) or infrared (IR) excitation, as well as their chemical and thermal stability.[7−17] Thus, orthoborate materials are applied for the color plasma display panels and used in Hg-free fluorescent lamps in view of an exceptionally optical damage threshold.[18,19]

In 1961 Levin et al. characterized three elementary crystal structures of REBO$_3$ doped with Ln^{3+} analogous to three crystalline forms of CaCO$_3$, which are associated with the ionic

radius of the rare earth. These are aragonite, calcite, and vaterite. The smallest rare earth ions (Sm to Yb) and yttrium borates crystallize in the vaterite-type form.[20] Then, in 1972 Meyer et al. proposed the high-temperature forms of LnBO$_3$ (Ln = Pr, Nd, Sm, Eu, Gd, Tb, and Dy), which crystallize in the triclinic system.[21] The first description of a triclinic crystal structure was published for SmBO$_3$ in 1976 by Palkina et al.[22] It was determined as a noncentrosymmetric space group $P1$. Then, over 20 years later, Corbel et al. characterized crystal structure of L-EuBO$_3$ as a centrosymmetric space group $P\bar{1}$.[23] Later, Huppertz et al. described a triclinic structure with a $P\bar{1}$ space group assigned to χ-DyBO$_3$ and χ-ErBO$_3$.[24] In this structure, the [B$_3$O$_9$]$^{9-}$ units do not create a ring and are formed from one BO$_3$ triangle and two BO$_4$ tetrahedrons. More recently, Noirault et. al presented the structure characterization of triclinic L-NdBO$_3$ with the centrosymmetric $P\bar{1}$ space group.[25] In the present work, the hydrothermal conditions were

used to prepare $Gd_{1-x}Eu_xBO_3$ nanoparticles, which crystallized in a new structure, characterized as a triclinic crystal system. Until now, the crystallographic data and detailed analysis of the structure of triclinic $GdBO_3$ were not published.

Known hexagonal rare earth orthoborates doped with Eu^{3+} ions exhibit red or orange-red luminescence under UV excitation. The characteristic emission spectra of $REBO_3:Eu^{3+}$ consist mainly of two almost equal transition bands, a typical magnetic dipole transition $^5D_0-^7F_1$ (orange) and a typical electric dipole transition $^5D_0-^7F_2$ (red). Therefore, the $REBO_3:Eu^{3+}$ phosphors present an orange-red emission instead of red one, and their chromaticity is poor, that limits their application.[26,27] As is well-known, the $^5D_0-^7F_2$ transition is hypersensitive to the symmetry of the crystal field around Eu^{3+} ions, and the intensity of the related emission band is high if the symmetry is low. In other words, when the Eu^{3+} ions are located in the inversion sites, the $^5D_0-^7F_1$ transition is allowed, while the $^5D_0-^7F_2$ transition is forbidden, that is the reason of the poor color purity.[28] Consequently, the structure of the $REBO_3:Eu^{3+}$ nanocrystals strongly influences their spectroscopic properties. Therefore, to overcome the problem of the low chromaticity, the symmetry of the crystal field should be reduced. It can be achieved through the synthesis of the nanosized $REBO_3:Eu^{3+}$ phosphors because, with the decreasing of the particle size, the number of Eu^{3+} ions occupying the surface area with distortion of inversion symmetry is increased.[15,29−31] Another way to obtain a pure red emission is the development of a material with a crystal structure, in which dopant ions occupy sites with low-symmetry environment. These two possibilities of reducing crystal field symmetry were used in the presented work.

The hydrothermal method is one of the most promising ways of materials synthesis, that allows controlling growth, and, hence, obtaining uniform and nonagglomerated nanocrystals. By monitoring the reaction parameters, such as the duration of synthesis and temperature, pure and homogeneous products can be obtained. Commonly, the additional reagents or templates, e.g., urea, ethylenediaminetetraacetic acid (EDTA), cetyldimethylammonium bromide (CTAB), or ethylene glycol, were used in order to obtain nanosized crystals with high homogeneity and uniformity.[27,29,32] Moreover, in most cases the precipitation of the precursor in the presence of NH_4OH or NaOH occurs before placing the colloidal solution or precipitate in the autoclave. Hence, in fact the formation reaction of nanoproducts starts without the hydrothermal conditions.[27,33−35]

In our experiment, a slightly modified hydrothermal reaction was employed in order to synthesize the $Gd_{1-x}Eu_xBO_3$ nanocrystals without any additional coreagents and templates. These nanomaterials were obtained *in situ*, by using the suitable solutions of the acetate salts of Ln^{3+} ions and boric acid. According to our knowledge, there are no other reports about the synthesis of $GdBO_3$ that crystallized in the triclinic crystal system. The triclinic crystal structure of $GdBO_3$ is determined for the first time. Moreover, synthesis in hydrothermal conditions enables us to obtain triclinic $GdBO_3$ nanocrystallites, unlike other ways of synthesis, e.g., the Pechini sol−gel method.[12] Therefore, we have focused on the detailed determination of the new $GdBO_3$ structure obtained by the hydrothermal method.

■ EXPERIMENTAL SECTION

Synthesis. The starting materials Gd_2O_3 and Eu_2O_3 (Stanford Materials, 99.99%) were dissolved in concentrated acetic acid (Chempur, pure p.a.). The obtained $Gd(CH_3COO)_3$ and $Eu-(CH_3COO)_3$ solutions were diluted with distilled water, and 0.25 M solutions were obtained. Then, the stoichiometric amounts (based on the formula $Gd_{1-x}Eu_xBO_3$, where the molar ratio was $x = 0-0.1$) of appropriate acetate salts and 0.5 M solution of H_3BO_3 (POCh S.A., p.a. grade) with 25% excess were mixed. Finally deionized water was added to the above mixture to rich 70 mL for the total volume of H_2O solution (pH ∼ 6.5). The as-obtained mixture was transferred to an autoclave and heated at 180 °C for 5 h. Afterward it was slowly cooled to room temperature. The synthesized nanocrystals were collected by centrifugation and washed with ethanol for several times. As-prepared white material was dried at 80 °C for 8 h in air.

Apparatus. X-ray diffraction patterns (XRD) were registered using a Bruker AXS D8 Advance diffractometer in Bragg−Brentano geometry, with Cu $K_{\alpha1}$ radiation (1.541 874 Å) in the 2θ ranges from 6° to 100°. Rietveld refinement was done with help of the Maud 2.0 software.[36,37]

TEM images and EDX spectra were recorded at a FEI Tecnai G2 20 X-TWIN transmission electron microscope, by an accelerating voltage of 200 kV.

The IR absorption spectrum was recorded between 400 and 4000 cm^{-1} on a FTIR spectrophotometer, Bruker FT-IR IFS 66/s. The material was mixed with KBr and then pressed into discs.

The Raman spectrum was registered using an Ar^+ laser (Stabilite 2017) operating at 514 nm and 7 mW at the sample. The scattered light was analyzed by a LabRAM HR800 (HORIBA Jobin Yvon) spectrometer.

The luminescence characteristics of the synthesized samples were studied with a Hitachi F-7000 fluorescence spectrophotometer at room and liquid nitrogen temperatures (300 and 77 K) with a 150 W xenon lamp as an excitation source. Excitation and emission spectra were corrected for the instrumental response.

The synchrotron radiation study of powder samples was performed at the SUPERLUMI station of HASYLAB, Hamburg, Germany. The setup has been described in detail elsewhere.[38] Luminescence spectra with resolution 1 nm were recorded with a SpectraPro308i (Acton) spectrograph equipped with a CCD camera. The second arm of the spectrograph equipped with a Hamamatsu photomultiplier R6358P was used for measuring the excitation spectra of different emission lines. In the latter case, the slits of the spectrograph were set for a spectral interval of 10 nm. The excitation spectra were corrected for the spectral distribution of incident light.

■ RESULTS AND DISCUSSION

Structure and Morphology. The applied hydrothermal conditions, appropriate pressure and temperature, and the use of such reagents as acetate salts enabled us to prepare $Gd_{1-x}Eu_xBO_3$ nanocrystals with the new crystal structure previously unknown for $GdBO_3$ compound. In order to accurately determine the new structure and to calculate the crystallographic parameters the Rietveld analysis was used. The calculated profile presented in Figure 1 fits well the experimental data with residual value $R_w = 0.0337$. The synthesized product crystallized in the triclinic system with space group $P\bar{1}$. The crystallographic data and atomic parameters are summarized in Table 1.

Figure 2 presents schematically the crystal structure of triclinic $GdBO_3$ nanocrystals. Figure 2a shows the coordination environment of the two Gd1 and Gd2 ions that are both 8-fold coordinated.[25] Boron ions are coordinated by oxygen ions in the form of BO_3^{3-} triangles, which are presented in the projection along the c axis in Figure 2c.[39,40] It is well seen that BO_3^{3-} units create anion sheets. The Gd^{3+} ions occupy sites between the formed sheets (Figure 2d).[41]
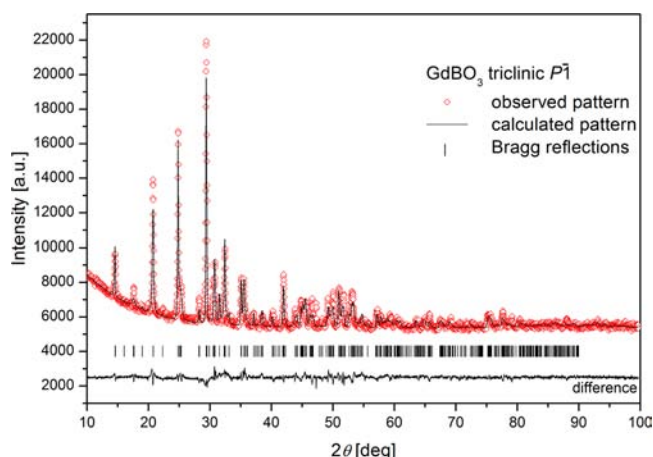
Figure 1. Rietveld profile fits of X-ray diffraction data of GdBO$_3$ dried at 80 °C for 8 h in air.

Table 1. Atomic Parameters for Triclinic GdBO$_3$

sample	GdBO$_3$, Z = 2	
space group	$P\bar{1}$ (2) triclinic	
cell parameters	a = 6.460(4) Å calcd	a = 6.493(1) Å ref[a]
	b = 6.464(8) Å calcd	b = 6.499(1) Å ref[a]
	c = 6.191(7) Å calcd	c = 6.242(1) Å ref[a]
	α = 107.874(4)° calcd	α = 107.79 (1)° ref[a]
	β = 108.379(9)° calcd	β = 107.42(1)° ref[a]
	γ = 92.714(3)° calcd	γ = 93.33(1)° ref[a]
	V = 230.77 Å^3 calcd	V = 236.04 Å^3 ref[a]
R	0.0224	
R_w	0.0337	
χ^2	0.0129	

atom	Wyckoff positions	x	y	z	B_{iso}
Gd1	2i	0.845(2)	0.264(3)	0.053(4)	0.526(8)
Gd2	2i	0.285(6)	0.184(6)	0.562(8)	0.526(8)
B1	2i	0.770(9)	0.278(3)	0.493(1)	0.526(8)
B2	2i	0.736(6)	0.755(6)	0.984(2)	0.526(8)
O1	2i	0.479(2)	0.223(0)	0.947(6)	0.526(8)
O2	2i	0.227(1)	0.123(3)	0.159(9)	0.526(8)
O3	2i	0.653(6)	0.206(0)	0.634(8)	0.526(8)
O4	2i	0.121(6)	0.853(1)	0.618(0)	0.526(8)
O5	2i	0.235(7)	0.630(0)	0.525(3)	0.526(8)
O6	2i	0.853(4)	0.651(3)	0.083(9)	0.526(8)

[a]ISCD #40745 SmBO$_3$.

In order to confirm the presence of plane BO$_3^{3-}$ groups and the coordination of boron in the triclinic Gd$_{1-x}$Eu$_x$BO$_3$ nanocrystals, the IR transmittance spectrum of the GdBO$_3$ matrix was measured (Figure 3). The presence of several strong absorption bands can be clearly detected. The absorption bands in the region 1100 and 1400 cm^{-1} are connected with the asymmetric stretching of B−O in BO$_3^{3-}$ units. Moreover, the peak centered at 941 cm^{-1} originates from the symmetric stretching of B−O in BO$_3^{3-}$ groups. Additionally, the bands located in the region 700−800 cm^{-1} and below 670 cm^{-1} are assigned to the out-of-plane bending vibrations of B−O in BO$_3^{3-}$ units. On the basis of the IR spectrum analysis it is certain that boron atoms are in 3-fold coordination and the Gd$_{1-x}$Eu$_x$BO$_3$ structure consists of the BO$_3^{3-}$ groups.[8,42,43]

Another way of confirmation that the planar BO$_3^{3-}$ groups can be found in the Gd$_{1-x}$Eu$_x$BO$_3$ structure is a Raman
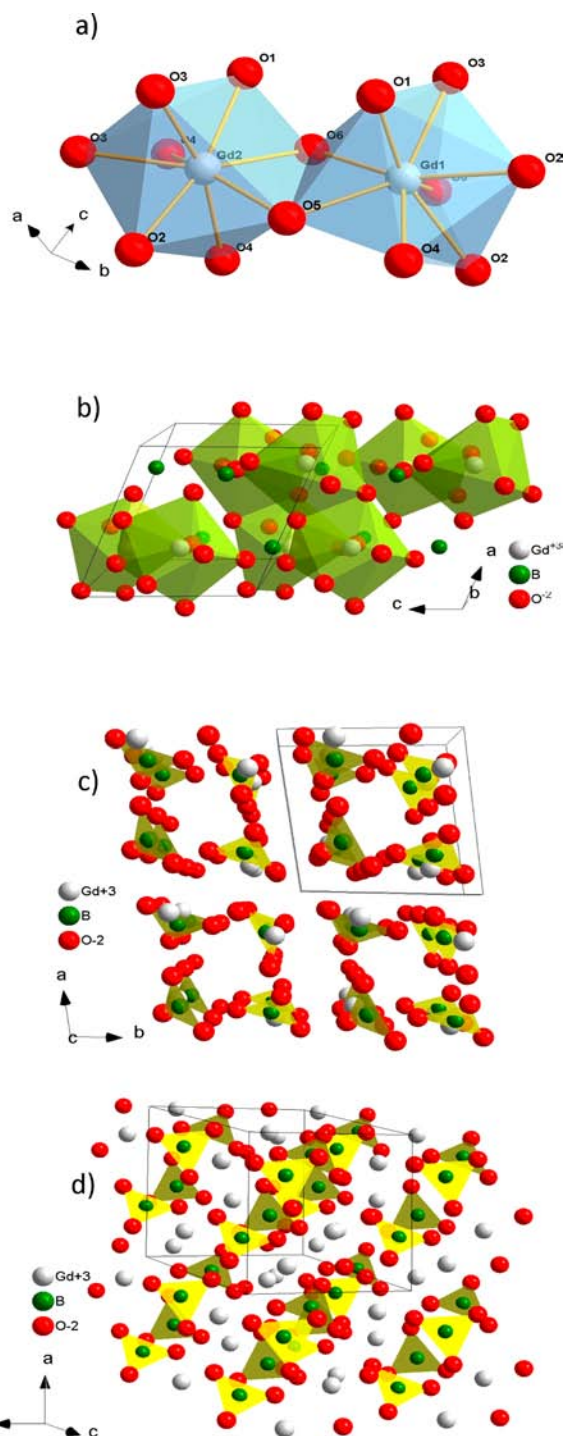
Figure 2. Structure of the triclinic GdBO$_3$ phase: (a) coordination environment of Gd1 and Gd2, (b) orientation arrangement of BO$_3^{3-}$ groups, (c) projection of the structure along the c-axis.

spectrum analysis (Figure 4). The highest energy phonon peak for the triclinic GdBO$_3$ was registered at 1310 cm^{-1}. This corroborates the role of the lighter trigonal BO$_3^{3-}$ borate group in triclinic GdBO$_3$, unlike GdBO$_3$ with monoclinic and rhombohedral crystallites, which consists of the heavier B$_3$O$_9^{9-}$ polyborate units, and for which, correspondingly, the highest energy phonon is observed near 1110 cm^{-1}.[12,14]

In Figure 5, XRD patterns of the nanosized Gd$_{1-x}$Eu$_x$BO$_3$ (x = 0−0.1) crystals are presented. The positions of all peaks are in good agreement with those in the pattern calculated for
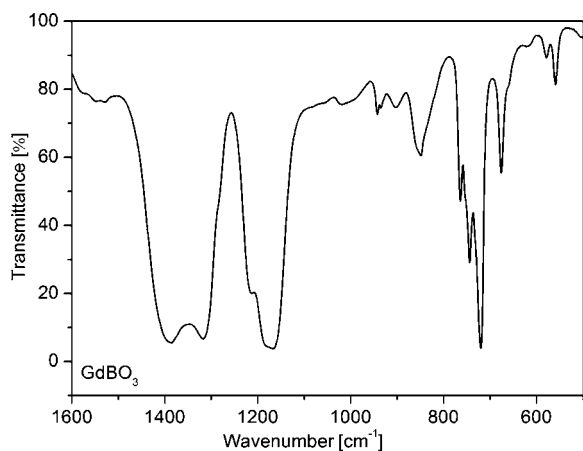
Figure 3. IR spectrum of undoped $GdBO_3$ dried at 80 °C for 8 h in air.
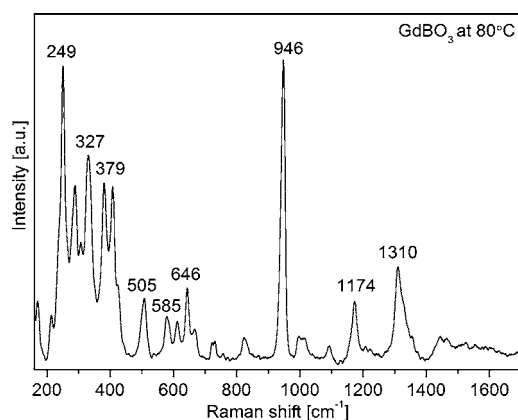
Figure 4. Raman spectrum of undoped $GdBO_3$ dried at 80 °C for 8 h in air.
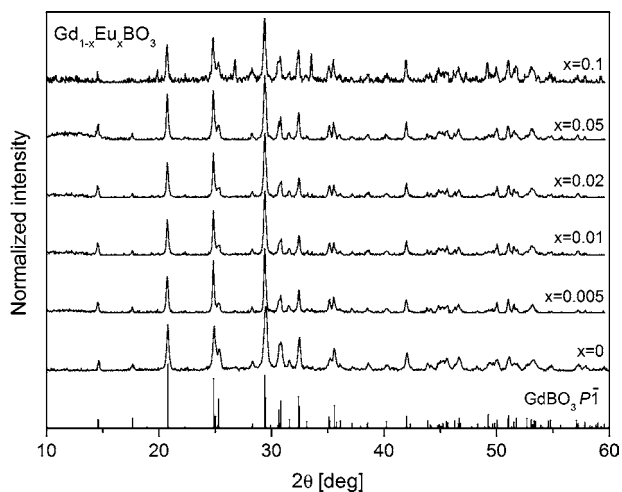
Figure 5. XRD patterns of the $Gd_{1-x}Eu_xBO_3$ ($x = 0-0.1$) nanocrystals dried at 80 °C for 8 h in air.

triclinic $GdBO_3$ with the $P\bar{1}$ space group. The results show that the pure phase of the triclinic $Gd_{1-x}Eu_xBO_3$ nanocrystals can be synthesized in the above-mentioned hydrothermal conditions without further calcination. The single-phase product with no presence of any additional peaks from extraneous admixtures was obtained in the whole range of the Eu^{3+} doping concentrations.

The size and morphology of the $Gd_{0.99}Eu_{0.01}BO_3$ nanoparticles was examined by transmission electron microscopy (TEM). As shown in Figure 6a−c, the nanoparticles are rodlike, and an average particle length is about 1 μm and width 20 nm.
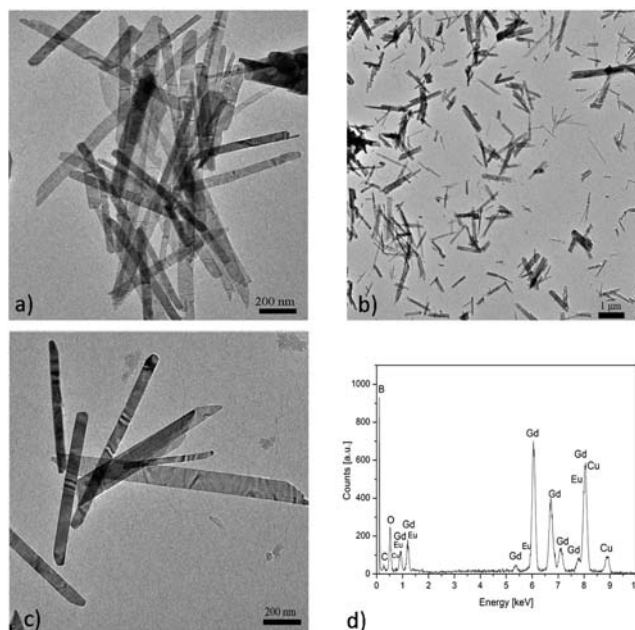
Figure 6. TEM images (a−c) and EDX spectrum (d) of the $Gd_{0.99}Eu_{0.01}BO_3$ nanocrystals dried at 80 °C for 8 h in air.

The EDX spectrum presented in Figure 6d confirms the presence of gadolinium, boron, oxygen, and europium in the stoichiometric composition. No impurities can be found. The EDX quantitative microanalysis proves the amount of 1% Eu^{3+} ions in the $GdBO_3$ phosphor.

The as-obtained $Gd_{1-x}Eu_xBO_3$ nanophosphors showed strong visible red emission under VUV and UV excitation due to the presence of the Eu^{3+} ions as luminescence centers in the structure. Figure 7 shows the excitation spectrum registered by using synchrotron radiation for the Eu^{3+} emission of $Gd_{0.99}Eu_{0.01}BO_3$ monitored at 616 nm. The spectrum consists
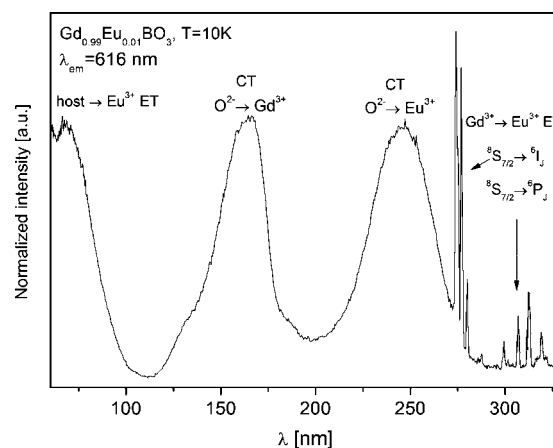
Figure 7. Excitation spectrum of $Gd_{0.99}Eu_{0.01}BO_3$ dried at 80 °C for 8 h in air measured at $T = 10$ K in the range of VUV and UV (host → Eu^{3+} ET-host lattice fundamental absorption/excitation band, Gd^{3+} → Eu^{3+} ET, Gd^{3+} f−f transitions).

of two intense and broad bands peaking at λ = 167 and 247 nm, which are ascribed to the charge transfer (CT) bands $O^{2-} \rightarrow Gd^{3+}$ and $O^{2-} \rightarrow Eu^{3+}$, respectively, and the onset at $\lambda < 100$ nm, which can indicate the energy transfer (ET) process from the host lattice to the Eu^{3+} ions.[9,44] The sharp and intense peaks located in the range from 274 to 325 nm correspond to the $^8S_{7/2} \rightarrow {}^6I_J$ and $^8S_{7/2} \rightarrow {}^6P_J$ transitions of Gd^{3+} ions.[10,45] This confirms that the energy transfer from Gd^{3+} to Eu^{3+} takes place efficiently.

Figure 8 shows the emission spectra of the $Gd_{0.99}Eu_{0.01}BO_3$, which consist of four main peak groups that are associated with
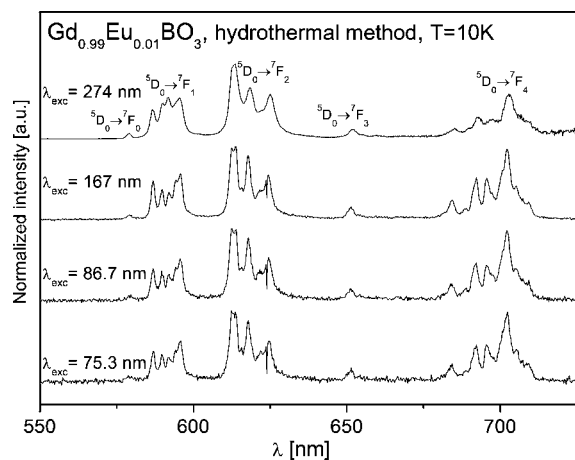
Figure 8. Emission spectra of $Gd_{0.99}Eu_{0.01}BO_3$ dried at 80 °C for 8 h in air registered under VUV and UV excitation.

the transitions from the excited $^5D_0$ level to ^7F_J ($J = 1-4$) levels of Eu^{3+} ions. The red emission band at 616 nm is more intense than the orange emission band at 594 nm. Hence, the chromaticity for this sample is improved, and the color is redder instead of common orange-red emission characteristic of borates. This agrees with the Eu^{3+} ion environment and morphology of nanorods that favors placing the Eu^{3+} ions on the nanoparticle surface, where the local symmetry is highly distorted. Generally, the intensity of the bands connected with transitions between different J levels is strictly related to the local site symmetry of the Eu^{3+} ions. On the basis of the selective rules, the magnetic dipole transitions are allowed, while the electric dipole transitions are forbidden. In a situation where Eu^{3+} ions occupy the sites with inversion symmetry, the intensities of the $^5D_0-{}^7F_1$ and $^5D_0-{}^7F_2$ transitions should be relatively high and low, respectively. In the opposite situation, i.e., the dopant ions are located in the C_1 site missing inversion symmetry, the probability of the $^5D_0-{}^7F_2$ transition increases.[13]

Moreover, by analyzing the emission spectrum, the relatively high ratio between the intensities of the $^5D_0-{}^7F_4$ transition band in relation to the $^5D_0-{}^7F_2$ peak could be observed. The intensity of the $^5D_0-{}^7F_4$ emission band is usually much lower, especially in the case of oxyfluorides and oxides.[5,46] Also, the ET band is quite intensely related to the CT bands in the excitation spectrum. This situation can be a result of the highly asymmetric and distorted environment of the Eu^{3+} ions.[47]

Figure 9 presents luminescence decay curves of $Gd_{1-x}Eu_xBO_3$ for different concentrations of Eu^{3+} ions ($x = 0.005-0.1$)
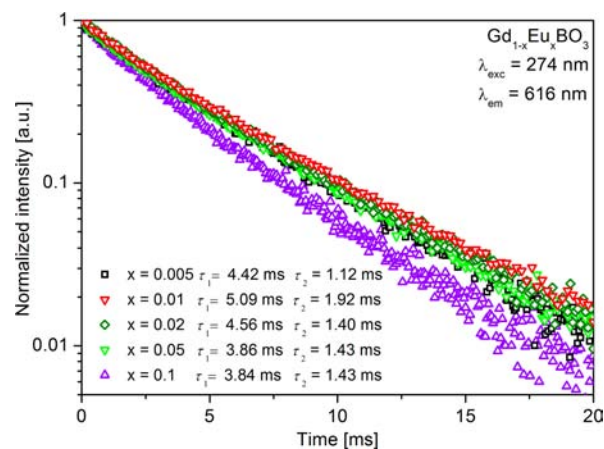
Figure 9. Decay curves of $Gd_{1-x}Eu_xBO_3$ dried at 80 °C for 8 h in air.

monitored at the maximum of the $^5D_0 \rightarrow {}^7F_2$ transition. All the decay curves can be well fitted by a biexponential function. Shorter components of the luminescent lifetimes are connected with the dopant ions located at the surface of crystallites, where the impact of the external environment is high and hence quenching of the excited states is strong. The luminescence lifetime is the longest for the 1% doped material and then shortens slightly with increasing dopant concentration in the $Gd_{1-x}Eu_xBO_3$ host. The reducing of the emission effective lifetimes can be connected with cross-relaxation between the Eu^{3+} ions.[30]

The Judd–Ofelt theory related to the 4f–4f transition intensities enables to define the character of the luminescence of Eu^{3+} ions by determining three intensity parameters Ω_2, Ω_4, and Ω_6 using a method described by Kodaira.[48] According to this method the $^5D_0 \rightarrow {}^7F_1$ transition performs as an internal standard that makes possible to calculate the radiative decay rates of the $^5D_0 \rightarrow {}^7F_2$ and $^5D_0 \rightarrow {}^7F_4$ transitions (A_{0-2} and A_{0-4}, respectively). The Einstein factors $A_{0-\lambda}$ can be calculated from the equation:

Table 2. Decay Rates of Radiative (A_{rad}), Nonradiative (A_{nrad}), and Total (A_{tot}) Processes of the $^5D_0 \rightarrow {}^7F_J$ Transitions, Luminescence Lifetimes Calculated by Fitting with a Biexponential Function (τ_1 and τ_2), and Their Amplitudes (A_1 and A_2), Effective Lifetimes (τ_{ef}), Intensity Parameters (Ω_2 and Ω_4), and Quantum Efficiencies (η) Determined from Spectroscopic Measurements of $Gd_{1-x}Eu_xBO_3$ Dried at 80°C for 8 h in Air

				lifetimes							
Eu^{3+}	A_{rad} (s^{-1})	A_{nrad} (s^{-1})	A_{tot} (s^{-1})	A_1	τ_1 (ms)	A_2	τ_2 (ms)	τ_{ef} (ms)	Ω_2 (10^{-20} cm^2)	Ω_4 (10^{-20} cm^2)	η (%)
$x = 0.005$	208	56	265	1303	4.42	199	1.12	3.78	8.8	11.3	78.8
$x = 0.01$	222	10	231	2733	5.09	957	1.92	4.32	9.6	12.2	95.8
$x = 0.02$	206	60	266	1771	4.56	375	1.40	3.76	8.9	10.5	77.5
$x = 0.05$	208	45	254	1092	3.86	330	1.43	3.24	10.2	10.8	76.4
$x = 0.1$	235	76	311	1047	3.84	317	1.43	3.22	8.8	13.6	75.6

$$A_{0-\lambda} = A_{0-J} = A_{0-1}\frac{I_{0-J}h\nu_{0-1}}{I_{0-1}h\nu_{0-J}} \tag{1}$$

where I_{0-J} and $h\nu_{0-J}$ represent the area under the spectral curve and the energy of the $^5D_0 \rightarrow {}^7F_\lambda$ transition. On the basis of the Judd−Ofelt theory, the Einstein coefficients of the spontaneous emission are formulated as:

$$A_{0-\lambda} = \frac{64\pi^4\nu^3e^2}{3hc^3}\frac{1}{4\pi\varepsilon_0}\chi\sum_{\lambda=2,4}\Omega_\lambda|\langle^5D_0\|U^{(\lambda)}\|^7F_J\rangle|^2 \tag{2}$$

The set of values determined for the $Gd_{1-x}Eu_xBO_3$ samples dried at 80 °C for 8 h in air are summarized in Table 2. The calculated Judd−Ofelt parameters are relatively high, that indicates a strong distortion of the Eu^{3+} local environment.[5,49−51] The Ω_2 parameter is especially sensitive to the local environment asymmetry of the Eu^{3+} site.[5] Also, the decrease in nanocrystal size can raise the value of this parameter.[49] The calculated Ω_4 parameters are relatively high, that can be caused by a low covalency of the chemical bond between Eu^{3+} and surrounding O^{2-} ions.[51] This parameter is not related directly to the symmetry of the Eu^{3+} ion but to the electron density on O^{2-} ions. It decreases when the electron density on surrounding ions increases.[50]

Moreover, it was noticed that η is the highest for $x = 0.01$. The quantities of the Eu^{3+} ions higher than $x = 0.01$ cause the reduced quantum efficiency probably due to cross-relaxation between the Eu^{3+} ions.[30]

CONCLUSIONS

The new triclinic structure of hydrothermally prepared $GdBO_3$ was determined using Rietveld refinement. Nanophosphors crystallized with the $P\bar{1}$ space group. The techniques used, such as XRD, IR, and Raman spectroscopy, confirmed the suggested structural properties. The electron microscopy (TEM) and EDX spectrum proved the formation of borate nanorods with the average particle length about 1 μm and width 20 nm. The luminescence properties were studied on the basis of the excitation and emission spectra and luminescence decay curves. Luminescence spectra present four the most intense peaks that are connected with the transitions from the excited $^5D_0$ level to the ^7F_J ($J = 1-4$) levels of Eu^{3+} ions. The luminescence decay curves of $Gd_{1-x}Eu_xBO_3$ monitored at the $^5D_0 \rightarrow {}^7F_2$ 616-nm transition were recorded and well fitted by a biexponential function. High luminescence efficiency of the $Gd_{1-x}Eu_xBO_3$ orthoborates makes them potentially useful for optical devices, e.g., panel display panels.

ASSOCIATED CONTENT

Ⓢ Supporting Information

Crystallographic data in CIF format. This material is available free of charge via the Internet at http://pubs.acs.org.

AUTHOR INFORMATION

Corresponding Author
*E-mail: blis@amu.edu.pl.
Notes
The authors declare no competing financial interest.

ACKNOWLEDGMENTS

REFERENCES

(1) Wang, X.; Zhuang, J.; Peng, Q.; Li, Y. *Nature* **2005**, *437*, 121−4.
(2) Li, X.; Gai, S.; Li, C.; Wang, D.; Niu, N.; He, F.; Yang, P. *Inorg. Chem.* **2012**, *51*, 3963−3971.
(3) Wiglusz, R. J.; Grzyb, T. *Opt. Mater.* **2011**, *33*, 1506−1513.
(4) Grzyb, T.; Lis, S. *J. Rare Earths* **2009**, *27*, 588−592.
(5) Grzyb, T.; Lis, S. *Inorg. Chem.* **2011**, *50*, 8112−20.
(6) Grzyb, T.; Szczeszak, A.; Rozowska, J.; Legendziewicz, J.; Lis, S. *J. Phys. Chem. C* **2012**, *116*, 3219−3226.
(7) Szczeszak, A.; Lis, S.; Nagirnyi, V. *J. Rare Earths* **2011**, *29*, 1142−1146.
(8) Lin, J.; Huang, Y.; Zhang, J.; Ding, X.; Qi, S.; Tang, C. *Mater. Lett.* **2007**, *61*, 1596−1600.
(9) Li, J.; Wang, Y.; Liu, B. *J. Lumin.* **2010**, *130*, 981−985.
(10) Chen, L.; Jiang, Y.; Chen, S.; Zhang, G.; Wang, C.; Li, G. *J. Lumin.* **2008**, *128*, 2048−2052.
(11) Dexpert-Ghys, J.; Mauricot, R.; Caillier, B.; Guillot, P.; Beaudette, T.; Jia, G.; Tanner, P. a.; Cheng, B.-M. *J. Phys. Chem. C* **2010**, *114*, 6681−6689.
(12) Szczeszak, A.; Grzyb, T.; Lis, S.; Wiglusz, R. J. *Dalton Trans.* **2012**, *41*, 5824−31.
(13) Wei, Z.; Sun, L.; Liao, C.; Yin, J.; Jiang, X.; Yan, C.; Lü, S. *J. Phys. Chem. B* **2002**, *106*, 10610−10617.
(14) Giesber, H.; Ballato, J.; Chumanov, G.; Kolis, J.; Dejneka, M. *J. Appl. Phys.* **2003**, *93*, 8987−8995.
(15) Kim, T.; Kang, S. *Mater. Res. Bull.* **2005**, *40*, 1945−1954.
(16) Yang, Z.; Yan, D.; Zhu, K.; Song, Z.; Yu, X.; Zhou, D.; Yin, Z.; Qiu, J. *Mater. Lett.* **2011**, *65*, 1245−1247.
(17) Giesber, H.; Ballato, J.; Pennington, W.; Kolis, J. *Inf. Sci.* **2003**, *149*, 61−68.
(18) Choi, S.; Park, B.-Y.; Jung, H.-K. *J. Lumin.* **2011**, *131*, 1460−1464.
(19) Ronda, C. R.; Jüstel, T.; Nikol, H. *J. Alloys Compd.* **1998**, *275−277*, 669−676.
(20) Levin, E. M.; Roth, R. S.; Martin, J. B. *Am. Mineral.* **1961**, *20*, 283−287.
(21) Meyer, H. J. *Naturwissenschaften* **1972**, *59*, 215−215.
(22) Palkina, K. K.; Kuznetsov, V. G.; Butman, L. A.; Dzhurinskii, B. F. *Coord. Chem. USSR* **1976**, *2*, 286−289.
(23) Corbel, G.; Leblanc, M.; Antic-Fidancev, E.; Lemaitre-Blaise, M.; Krupa, J. C. *J. Alloys Comp.* **1999**, *287*, 71−78.
(24) Huppertz, H.; Von der Eltz, B.; Hoffmann, R.-D.; Piotrowski, H. *J. Solid State Chem.* **2002**, *166*, 203−212.
(25) Noirault, S.; Joubert, O.; Caldes, M. T.; Piffard, Y. *Acta Crystallogr., Sect. E* **2006**, *62*, i228−i230.
(26) Yang, L.; Zhou, L.; Huang, Y.; Tang, Z. *Mater. Lett.* **2010**, *64*, 2704−2706.
(27) Zhang, J.; Lin, J. *J. Chem. Phys.* **2004**, *271*, 207−215.
(28) Guo, X.; Wang, Y.; Zhang, J. *J. Cryst. Growth* **2009**, *311*, 2409−2417.
(29) Jiang, X.; Yan, C.; Sun, L.; Wei, Z.; Liao, C. *J. Solid State Chem.* **2003**, *175*, 245−251.
(30) Yadav, R. S.; Dutta, R. K.; Kumar, M.; Pandey, A. C. *J. Lumin.* **2009**, *129*, 1078−1082.
(31) Wei, Z.; Sun, L.; Liao, C.; Yan, C.; Huang, S. *Appl. Phys. Lett.* **2002**, *80*, 1447.

(32) Yang, Z.; Wen, Y.; Sun, N.; Wang, Y.; Huang, Y.; Gao, Z.; Tao, Y. *J. Alloys Compd.* **2010**, *489*, L9−L12.

(33) Jiang, X.; Sun, L.; Feng, W.; Yan, C. *Cryst. Growth Des.* **2004**, *4*, 517−520.

(34) Jiang, X.; Sun, L.; Yan, C. *J. Phys. Chem. B* **2004**, *108*, 3387−3390.

(35) Xu, Z.; Li, C.; Cheng, Z.; Zhang, C.; Li, G.; Peng, C.; Lin, J. *CrystEngComm* **2010**, *12*, 549.

(36) Rietveld, H. M. *J. Appl. Crystallogr.* **1969**, *2*, 65−71.

(37) Lutterotti, L.; Bortolotti, M. *Compcomm. Newsletter* **2003**, *1*, 43−50.

(38) Zimmere, G. *Radiat. Meas.* **2007**, *42*, 859−864.

(39) Mączka, M.; Waśkowska, A.; Majchrowski, A.; Kisielewski, J.; Szyrski, W.; Hanuza, J. *J. Solid State Chem.* **2008**, *181*, 3211−3216.

(40) Yin, M.; Corbel, G.; Leblanc, M.; Antic-Fidancev, E.; Krupa, J. . *J. Alloys Compd.* **2000**, *302*, 12−15.

(41) Ren, M.; Lin, J. H.; Dong, Y.; Yang, L. Q.; Su, M. Z.; You, L. P. *Chem. Mater.* **1999**, *11*, 1576−1580.

(42) Lemanceau, S. *J. Solid State Chem.* **1999**, *148*, 229−235.

(43) Jia, G.; Zhang, C.; Wang, C.; Liu, L.; Huang, C.; Ding, S. *CrystEngComm* **2012**, *14*, 579.

(44) Xiangzhong, C.; Weidong, Z.; Xying, Z.; X, T.; Zhen, L.; Zhijian, Y.; Chunlei, Z.; Xiawoei, H. *J. Rare Earths* **2006**, *24*, 719−723.

(45) Wang, Y.; Endo, T.; He, L.; Wu, C. *J. Cryst. Growth* **2004**, *268*, 568−574.

(46) Wiglusz, R.; Grzyb, T.; Lis, S.; Strek, W. *J. Nanosci. Nanotechnol.* **2009**, *9*, 5803−5810.

(47) Sá Ferreira, R. a.; Nobre, S. S.; Granadeiro, C. M.; Nogueira, H. I. S.; Carlos, L. D.; Malta, O. L. *J. Lumin.* **2006**, *121*, 561−567.

(48) Kodaira, C. *J. Lumin.* **2003**, *101*, 11−21.

(49) Grzyb, T.; Węcławiak, M.; Lis, S. *J. Alloys Compd.* **2012**, *539*, 82−89.

(50) Tanabe, S.; Ohyagi, T.; Soga, N.; Hanada, T. *Phys. Rev. B* **1992**, *46*, 3305−3310.

(51) Tanabe, S.; Hanada, T.; Ohyagi, T.; Soga, N. *Phys. Rev. B* **1993**, *48*, 10591−10594.

4940

dx.doi.org/10.1021/ic302525k | *Inorg. Chem.* 2013, 52, 4934−4940